

# Motion Planning of Piezoelectrically Driven Micro-Robots via Navigation Functions\*

Savvas G. Loizou, Kostas J. Kyriakopoulos

*Control Systems Lab.*

*National Technical University of Athens*

*Athens, Greece*

*{sloizou,kkyria}@mail.ntua.gr*

**Abstract**—In this paper we present a closed loop switching control methodology applicable to piezoelectrically driven micro-robots whose locomotion principle is based on the stick slip effect. The derived controller has theoretically guaranteed global convergence and collision avoidance properties. The effectiveness of the proposed methodology is verified through hardware experiments and computer simulations.

**Index Terms**—micro-robots, navigation-functions, stick-slip, bounded-input, switching control

## I. INTRODUCTION

In recent years micro-systems technology and micro-robotics has evolved to an important scientific field with great application potential [8]. Motion planning for micro-robots is a field of special interest to micro-robotics, due to the specialized locomotion principles being used to drive the micro-robots and the need for special controllers to handle the micro-scale effects affecting their motion [19], [3].

Several solutions were provided for controlling a micro-robot. In [17], a machine learning based hierarchical object oriented control architecture using task primitives is presented for applications in micro-robot operations. In [16] a DSP based fuzzy logic control strategy is applied to control a micro-robot with biped structure. In [1] an on-line simulation environment for plan feasibility checking for micro-robots is presented. In [9] a control methodology is presented for actuating a micro robot using piezoelectric elements and electromagnets. In [13] a soft computing trajectory controller based on a neural network map trained by experimental data with the help of fuzzy rules was applied to micro walking robots with piezoelectric legs.

In this paper we tackle the issue of navigating a micro-robot in a workspace populated with obstacles. Depending on the piezoelectric driver design [3], [2], [14], even after calibration, the actuating mechanism "favors" certain motion directions, in the sense that the velocity error for a requested velocity across certain directions is significantly smaller than in other directions. This observation is a very important factor to consider when designing navigation and/or cooperative control methodologies for applications in micro-world task execution. The main contribution of this

paper is to use a navigation function [10] based feedback controller appropriately designed to actuate the micro-robot in the "favored" velocity directions, while maintaining the global convergence and collision avoidance properties of the navigation function.

The rest of the paper is organized as follows: Section II presents the preliminary notions while section III presents the theoretical controller synthesis procedure. Section IV presents the simulation results and section V presents the conducted experiment. The paper concludes with section VI.

## II. PRELIMINARIES

### A. Platform Description

In order to experimentally investigate as early as possible the nonuniform character of the motion principle exhibited by such type of actuators, we used as an early prototype the MINIMAN III platform [7], [18], [5], [6] shown in figure 1, as the MiCRoN [20] prototypes were not fully functional at the time of experimentation. Both of those prototypes exhibit the decoupled  $x$ ,  $y$  and  $\theta$  directions as their "favored" motion directions. Figure 2 shows a contour of the velocity error when actuating in  $x$ - $y$  directions. Notice here that the velocity error is significantly smaller for actuation in decoupled directions, while increasing fast for actuation in mixed directions.

The adopted MINIMAN III micro-positioning unit uses 3 tube-shaped piezo-legs for actuating in two translational ( $x$  and  $y$ ) and a rotational direction ( $\theta$ ) using the stick-slip effect [4]. The maximum achievable speed of the micro-robot is 30 mm/s. A global positioning CCD camera provided position estimates of the system based on a Kalman Filter estimator.

### B. Kinematics

Figure 3 depicts the coordinate systems we are about to use for modeling the system. The robot dynamics and actuator non-linearities are compensated through the use of machine learning methodologies [6]. Hence in our approach we only need to consider the kinematic model of the robot. The kinematics of the micro-robotic platform we are considering can be described as:

$$\dot{\mathbf{q}} = \mathbf{v} + \mathbf{e}_r(\mathbf{v}) \quad (1)$$

\* The authors want to acknowledge the contribution of the European Commission through contract IST – 2001 – 33567 – MICRON and IST – IP – 507006 – ISWARM

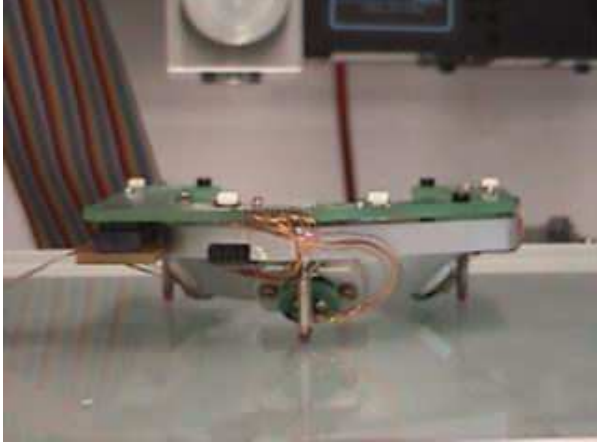


Fig. 1. The MINIMAN III positioning unit

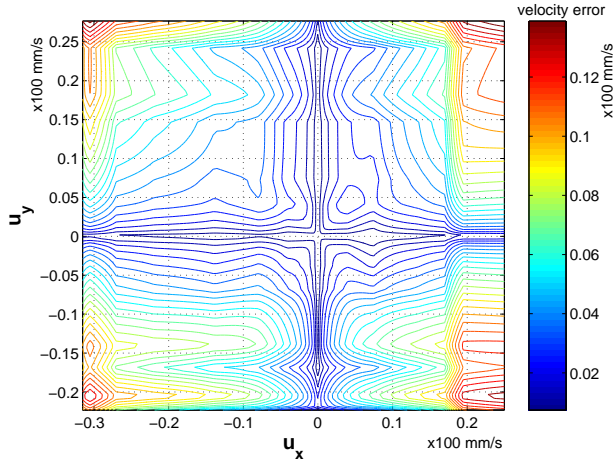


Fig. 2. Contour lines of the velocity error when actuating in x-y directions

where  $\mathbf{q} = [x \ y \ \theta]^T$  is the robot position,  $\dot{\mathbf{q}}$  is the performed velocity by the robot,  $\mathbf{v} = [v_x \ v_y \ w]^T$  is the requested robot velocity and  $\mathbf{e}_r(\mathbf{v}) = [e_{r_x}(\mathbf{v}) \ e_{r_y}(\mathbf{v}) \ e_{r_\theta}(\mathbf{v})]^T$  is the velocity error function. This error is due to micro-scale effects affecting the actuation mechanism, causing the input velocity to be different from the actual, and is characteristic for each micro-robot. In the following analysis we will use  $u_\theta = w$  for notational consistency. Let

$$\mathbf{u} = [u_x \ u_y \ u_\theta]^T = R^T(\theta) \mathbf{v}$$

be the robot velocities wrt the body fixed frame, where the rotation matrix is defined as:

$$R(\theta) = \begin{bmatrix} \cos(\theta) & -\sin(\theta) & 0 \\ \sin(\theta) & \cos(\theta) & 0 \\ 0 & 0 & 1 \end{bmatrix}$$

For the error function, it holds that

$$\mathbf{e}_r(\mathbf{v}) = R(\theta) \mathbf{e}(\mathbf{u})$$

i.e. it is invariant under rotation wrt the body fixed frame.  $\mathbf{e}(\mathbf{u}) = [e_x(\mathbf{u}) \ e_y(\mathbf{u}) \ e_\theta(\mathbf{u})]^T$  is a nonlinear function of

$\mathbf{u}$  and as can be seen from figure 2, the velocity error:  $\|\mathbf{e}\|$  increases very slowly across the decoupled motion directions, that is across  $u_x$ ,  $u_y$  or  $u_\theta$  (not shown in graph), which are the so called "favored" directions. This observation lead us to consider the following kinematic model for our system:

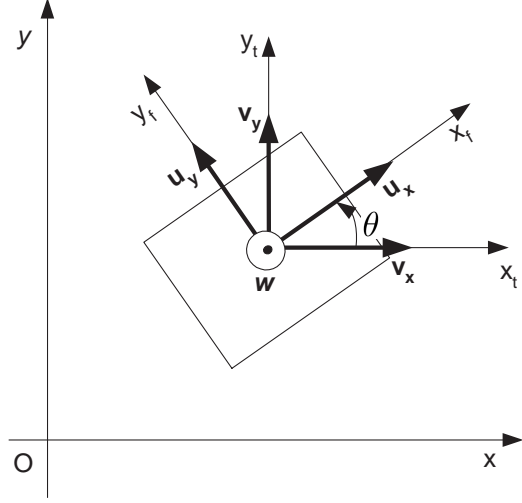


Fig. 3. Coordinate systems

$$\dot{\mathbf{q}} = R(\theta) (\mathbf{u} \circ \sigma + \mathbf{e}(\mathbf{u} \circ \sigma)) \quad (2)$$

where

$$\sigma \in \left\{ \sigma_x = \begin{bmatrix} 1 \\ 0 \\ 0 \end{bmatrix}, \sigma_y = \begin{bmatrix} 0 \\ 1 \\ 0 \end{bmatrix}, \sigma_\theta = \begin{bmatrix} 0 \\ 0 \\ 1 \end{bmatrix} \right\}$$

The  $\circ$  operator is the Hadamard (or Schur) product. For the matrices  $A = [a_{ij}]$ ,  $B = [b_{ij}] \in \mathbb{R}^{m \times n}$ , the Hadamard product of  $A$  and  $B$  is  $A \circ B = [a_{ij}b_{ij}]$ .

This kinematic model allows actuation in only pre-specified directions that belong in the set  $\sigma$ . This way we can actuate the micro-robotic system in the "favored" directions, incurring minimum error over the performed velocity at every actuation.

We need to actuate the micro-robot in the region of velocities where the velocity error in any direction is just a fraction of the requested velocity. We can thus define the maximum velocity  $u^{\max} = [u_x^{\max} \ u_y^{\max} \ u_\theta^{\max}]^T$  in the following way:

$u_j^{\max}$  is such that the following relations hold:

$$\forall |u_j| < u_j^{\max} \Rightarrow |e_i(\mathbf{u} \circ \sigma_j)| < c_{ij} |u_j|, \forall i, j \in \{x, y, \theta\} \quad (3)$$

with

$$c_{ij} > 0, \quad \sum_{i \in \{x, y, \theta\}} c_{ij} < 1, \forall j \quad (4)$$

If equation (3) holds for all  $u_j$ , then  $u_j^{\max}$  can be chosen so the system satisfies other constraints i.e. maximum power consumption, sensing rate, communication bandwidth, maximum platform achievable velocity. Obviously if  $u_j^{\max}$  satisfying conditions (3) and (4) cannot be found, that means

that the error is always greater than the input velocity and the proposed methodology cannot be applied. Experimental data (figure 4) for the micro-robotic platform verify our way of defining  $u_i^{\max}$  from equation (3), since velocity errors lie below the  $0.3u_x$  line hence there can be choices for  $c_{ij}$  satisfying inequalities (4).

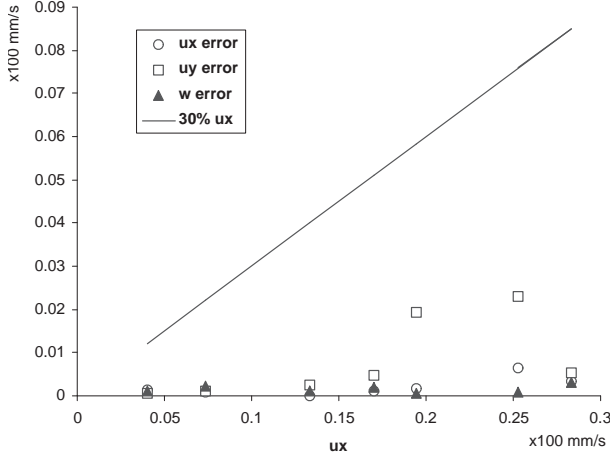


Fig. 4. Velocity error when actuating in x direction

### C. Navigation Functions

Navigation functions [10] are a special category of potential functions. They are smooth real valued maps from  $\mathbb{R}^n$  to  $\mathbb{R}$  which attain their maximum over the workspace boundary and have a unique minimum at the system's destination point. Any world that is diffeomorphic to a sphere world can be handled by navigation functions [15]. Navigation functions can be used as Lyapunov function candidates. We will use  $\varphi(\mathbf{q})$  to denote a navigation function. The flows of the negated gradient vector field of a navigation function:

$$\dot{x} = -\nabla\varphi$$

are globally asymptotically stable at the destination point for almost all initial conditions except a set of measure zero of initial conditions that lead the system to saddle points. Since those initial conditions are sets of measure zero (with an unstable sub-manifold) the possibility of starting in such a set is zero. It has been shown [10] that topological restrictions prohibit the creation of a globally attractive equilibrium in a sphere world populated with obstacles and that the best one can achieve with a smooth vector field is to have at least as many saddles as obstacles. Using a control law which is stable in the Lyapunov sense, with a Navigation Function as a Lyapunov function candidate, guarantees that the system will have global convergence, since Navigation Functions have one unique minimum and collision avoidance properties, since the workspace boundary (which includes obstacle perimeters) is repulsive. The interested reader can refer to [10] for more details on Navigation Functions. Navigation function methodologies assume a static environment with

global knowledge of the environment and the system. The authors of this paper have extended the navigation function methodology [11], [12] to the case of multiple robots. The methodology presented in this paper can be readily applied to multirobot scenarios by using MRNFs [11], [12] (Multi-Robot Navigation Functions).

### III. CONTROLLER SYNTHESIS

The problem we are considering in this paper can be stated as follows: *Derive a feedback kinematic control law that drives system (2) from any initial configuration to a target configuration avoiding collisions. The workspace is considered known, static and bounded.*

*Proposition 1:* System (2) under the control law

$$\mathbf{u} \circ \sigma = -u^{\max} \circ \frac{R(\theta)^T \nabla\varphi}{a + \left| \left( R(\theta)^T \nabla\varphi \right) \cdot \sigma_j \right|} \circ \sigma_j \quad (5)$$

where  $a > 0$  a parameter,  $\varphi = \varphi(\mathbf{q})$  is a navigation function and

$$j = \arg \max_{i \in \{x, y, \theta\}} \left( \left| \left( R(\theta)^T \nabla\varphi \right) \cdot \sigma_i \right| \right)$$

is globally asymptotically stable a.e.<sup>1</sup>

*Proof:* We will use the Navigation function  $V = \varphi$  as a Lyapunov function candidate. Taking the time derivative of  $V$  across the system's (2) trajectories, we get:

$$\dot{V} = \frac{\partial V}{\partial t} + \dot{\mathbf{q}}^T \cdot \nabla V = \dot{\mathbf{q}}^T \cdot \nabla V$$

since the environment is static. Substituting  $\dot{\mathbf{q}}$  from equation (2), we get:

$$\begin{aligned} \dot{V} &= (R(\theta) (\mathbf{u} \circ \sigma + \mathbf{e}(\mathbf{u} \circ \sigma)))^T \cdot \nabla\varphi \\ &= -\frac{u_j^{\max} R(\theta)^T \nabla\varphi \circ \sigma_j}{a + R(\theta)^T \nabla\varphi \cdot \sigma_j} + \mathbf{e}(\mathbf{u} \circ \sigma) \cdot R(\theta)^T \nabla\varphi \end{aligned}$$

Using the inequalities (3), we get:

$$\begin{aligned} \dot{V} &\leq -\frac{u_j^{\max} R(\theta)^T \nabla\varphi \cdot \sigma_j^2}{a + R(\theta)^T \nabla\varphi \cdot \sigma_j} + \dots \\ &\dots + \frac{c_{ij} u_j^{\max} R(\theta)^T \nabla\varphi \cdot \sigma_j R(\theta)^T \nabla\varphi \cdot \sigma_i}{a + R(\theta)^T \nabla\varphi \cdot \sigma_j} \end{aligned}$$

Form the control law of Proposition 1, we have that

$$R(\theta)^T \nabla\varphi \cdot \sigma_j \geq R(\theta)^T \nabla\varphi \cdot \sigma_i$$

hence:

$$\dot{V} \leq -\frac{u_j^{\max} R(\theta)^T \nabla\varphi \cdot \sigma_j^2}{a + R(\theta)^T \nabla\varphi \cdot \sigma_j} \left( 1 - \frac{c_{ij}}{i \in \{x, y, \theta\}} \right)$$

Using equation (4), we get:

$$\dot{V} \stackrel{a.e.}{<} 0$$

<sup>1</sup>a.e.:almost everywhere, i.e. everywhere except a set of initial conditions of measure zero

that is  $\dot{V}$ , away from the destination, is negative everywhere except a set of measure zero of initial conditions that lead to saddle points ■

We can also state the following:

*Corollary 1:* The control law defined in Proposition 1 satisfies the input constraints:

$$|u_i| \leq |u_i^{\max}|, \forall i \in \{x, y, \theta\}$$

*Proof:* From equation (5) we have that

$$\|\mathbf{u} \circ \sigma\| = |u_j| = u_j^{\max} \frac{|R(\theta)^T \nabla \varphi \cdot \sigma_j|}{a + |(R(\theta)^T \nabla \varphi) \cdot \sigma_j|} \leq u_j^{\max}$$

since  $\frac{|x|}{a+|x|} \leq 1, \forall a > 0, x \in \mathbb{R}$  ■

#### IV. SIMULATION

Before carrying out experiments with the actual hardware, a simulation was set up to verify the feasibility of the proposed control scheme. The simulation setup consisted of a spherical workspace with three obstacles. We carried out two simulations. In the first simulation the robot was actuated in the whole actuation space, i.e. the system's kinematics were described by equation (1) with  $\dot{\mathbf{v}} = -\nabla \varphi$  and in the second simulation the robot was actuated only in the favored velocity regions, i.e. equation (2) under the control law (5). The error function was simulated by a random vector with uniform radial distribution whose norm followed a normal distribution with mean value as shown in figure 2 for each actuation and variance equal to the one third of this mean value. We used the same initial and final configurations for both simulations. Figures 5a. and 5b. show the resulting trajectories for each simulation. As can be seen from figure 5a., the trajectory when actuating in the whole actuation space is more jerky. In the region near the obstacle where we have higher input velocities – especially in the mixed velocity directions (see figure 2) – this is very intense. When using the controller (5), the resulting trajectory (figure 5b.) is much smoother.

Figures 6a. and 6b. show the distance of the robot's reference point from the target position versus time. One can see the convergence properties of the system with the controller (5) (fig. 6b.) vs the system without the controller (fig. 6a.). Those figures are shown in logarithmic scale, to emphasize the behavior near the destination, since we are especially interested in achieving as much positioning accuracy as possible.

As can be seen the system actuating in only the favored velocity directions is stabilized at the target with an accuracy higher than  $10^{-10}m$ , while the system actuating in the whole actuation region fluctuates at a distance of  $10^{-5}m$  around the destination. Figure 7 shows the actuations that took place during the two simulations.

#### V. EXPERIMENT

##### A. Experimental setup

To verify the efficiency of the proposed methodology we carried experiments at the Institute for Process Control and

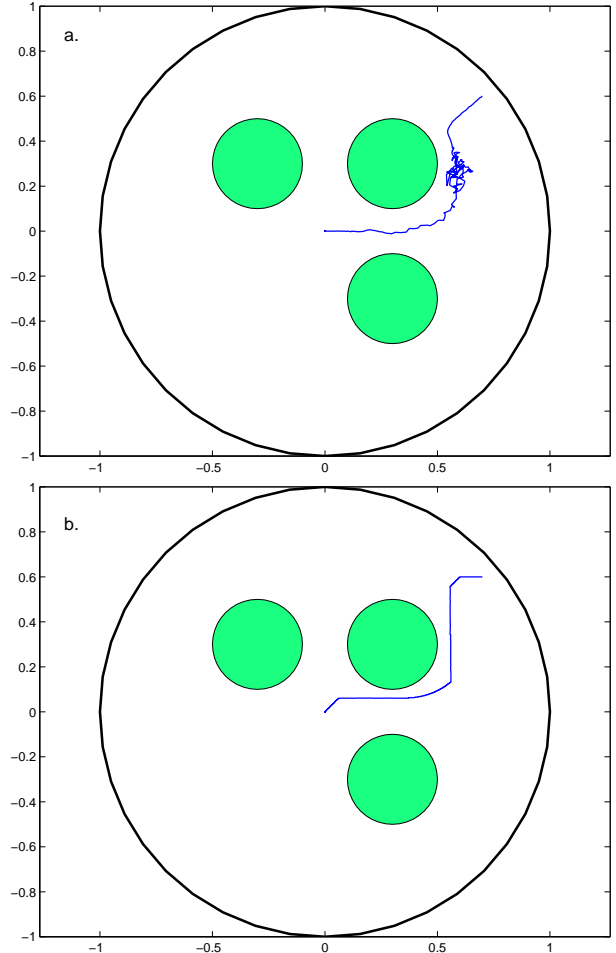


Fig. 5. Resulting simulation trajectories when actuating in (a.) the whole actuation space and (b.) in the 'favored' actuation directions

Robotics (IPR) of the University of Karlsruhe (Germany) and used the experimental setup depicted in figure 8. The setup consisted of a MINIMAN III [18] micro-positioning unit and an immobilized (due to the lack of position feedback at the time of experimentation) MiCRoN [20] robot, that served as an obstacle in the experiment.

A CCD camera positioned on top of the workspace provided position estimation for the MINIMAN III robot, based on position measurements of the four robot mounted LEDs. As commented earlier the two micro-robotic platforms (MINIMAN III and MiCRoN) exhibit similar behavior regarding the "favored" regions (i.e. the  $\sigma$  set of the MINIMAN III positioning unit is a subset of the  $\sigma$  set of the MiCRoN robot), hence the methodology should be readily applicable to the MiCRoN platform.

##### B. Execution

A navigation function was setup containing the workspace boundary which was defined by the portion of the workspace in which the CCD camera was providing estimates. The accuracy of the camera measurements was of the order of  $100\mu m$ . A circular disk over-approximating

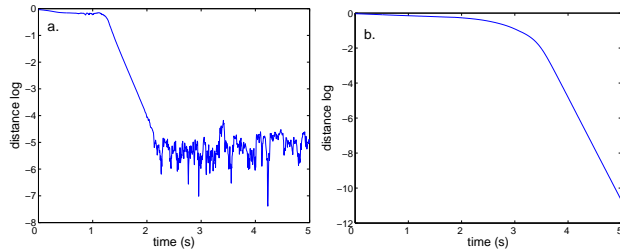


Fig. 6. Distance to the target logarithm for the resulting simulation trajectories when actuating in (a.) the whole actuation space and (b.) in the 'favored' actuation directions

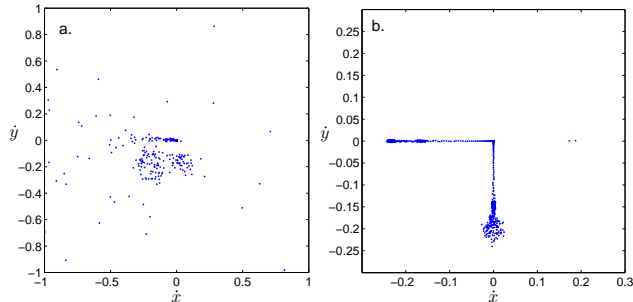


Fig. 7. Actuations performed during simulation when actuating in (a.) the whole actuation space and (b.) in the 'favored' actuation directions

the circumference of the MiCRoN robot was modeled in the navigation function. The MINIMAN III positioning unit was placed at it's initial position shown in figure 9 and it's target was set at the origin (fig. 10-d.). The system was programmed to stop after reaching at a distance of at most  $100\mu\text{m}$  from the destination.

Figure 10 depicts several snapshots from the experiment execution

Figure 11 depicts the distance to the target during the execution. Based on the Kalman filter estimate, the distance from the target when the robot stopped was  $62\mu\text{m}$ .

## VI. CONCLUSIONS

We successfully implemented a navigation function based closed form feedback controller for the task of navigating a piezoelectrically driven micro-robotic platform. The proposed controller has theoretically guaranteed global convergence and collision avoidance properties. This controller takes into account the "favored" velocity directions of the micro-robot - that is the velocity directions across which the velocity error is minimal - and achieves that way to converge asymptotically to the specified destination, avoiding collisions. In addition to the theoretical guarantees, an experimental application of the proposed controller verified the effectiveness of the proposed control scheme. The proposed controller can be readily applied to multi-robot navigation scenarios, using multi-robot navigation functions (MRNFs) [11], [12].

Further research includes expanding the methodology to arbitrarily many "favored" half-directions for actuation, as initial results from a neural network training of the robot

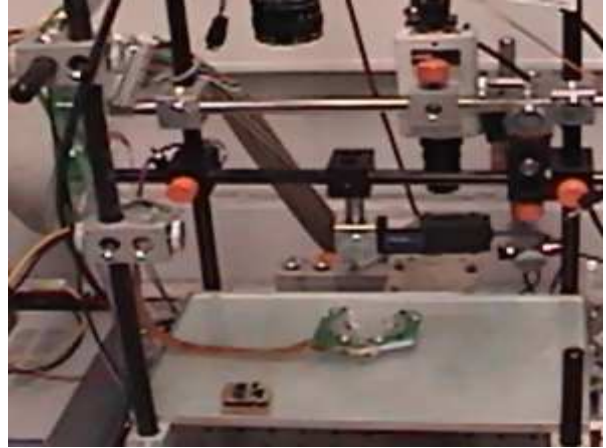


Fig. 8. Experimental setup



Fig. 9. Initial position

driver subsystem indicate a possibility for creating additional "favored" actuation half-directions or even favored actuation regions - i.e. regions where the velocity error is significantly smaller. Utilization of those additional regions and half-directions, given appropriate control design, will enable faster convergence of the system and additional capability to perform cooperative tasks.

**Acknowledgements:** The authors would like to thank Michael Thiel and the rest of the IPR MiCRoN team for their help during setting up and carrying out the experimental process.

## REFERENCES

- [1] H. Aoyama, M. Nozue, F. Iwata, J. Fukaya, and A. Sasaki. Navigation and formation control for distributed miniature robots with micro tool and sensor. *Int. Symp. on Micro Machine and Human Science*, pages 255–260, 1995.
- [2] A. Bergander and J.-M. Breguet. Performance improvements for stick-slip positioners. *IEEE MHS*, pages 59–66, 2003.
- [3] A. Bergander, W. Driesen, T. Varidel, and J.-M. Breguet. Monolithic piezoelectric actuators for miniature robotic systems. *ACTUATOR 2004*, 2004, Bremen, Germany.

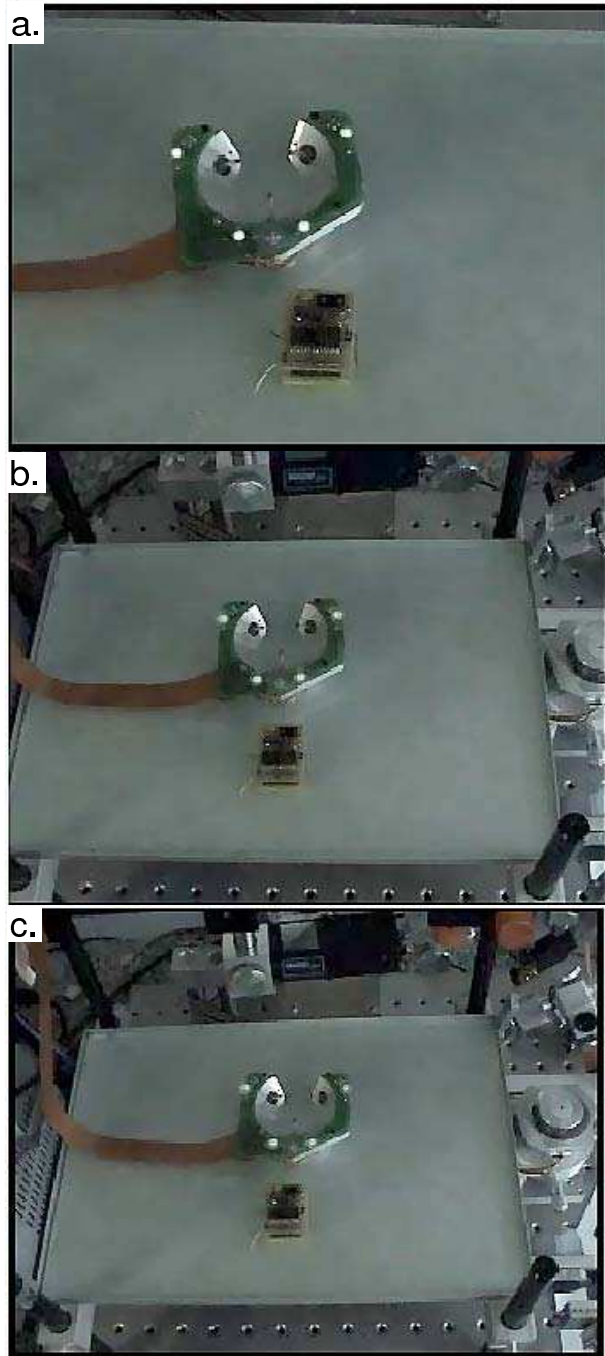


Fig. 10. Intermediate and final configurations

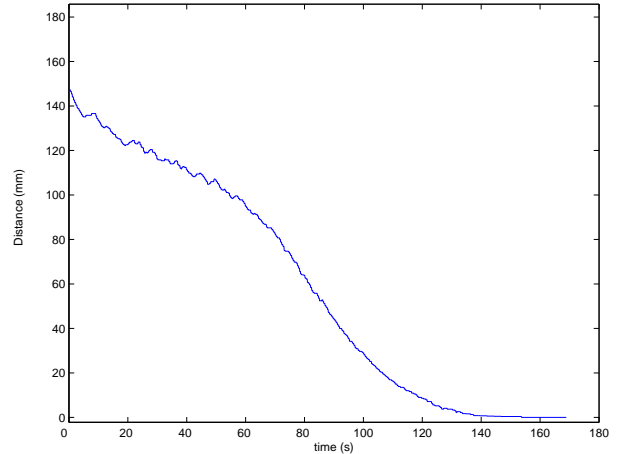


Fig. 11. Distance to the target

- [4] J.-M. Breguet, E. Pernette, and R. Clavel. Stick and slip actuators and parallel architectures dedicated to micro-robotics. *Proc. SPIE 2906*, pages 13–24, 1996.
- [5] J. Domingo, M. Puig-Vidal, J. López, and J. Samitier. Non linear control system based in fuzzy logic technique applied to drive piezoactuators for micro robotic applications miniman: Miniaturized robot for micro manipulation. *IEEE Int. Conf. on Emerging Tech. and Factory Automation*, pages 559–563, 1999.
- [6] R. Estana, J. Seyfried, F. Schmoekkel, M. Thiel, A. Buerkle, and H. Woern. Exploring the micro- and nanoworld with cubic centimetre-sized autonomous microrobots. *Industrial Robot*, 31(2):159–178, 2004.
- [7] S. Fahlbusch, S. Fatikow, J. Seyfried, and A. Buerkle. Flexible microrobotic system miniman: Design, actuation principle and control. *IEEE/ASME Int. Conf. on Adv. Int. Mechatronics*, pages 156–161, 1999.
- [8] S. Fatikow and U. Rembold. *Microsystem Technology and Microrobotics*. Springer, 1997.
- [9] R. Fukui, A. Torii, and A. Ueda. Micro robot actuated by rapid deformation of piezoelectric elements. *Int Symp. on Micromechanics and Human Science*, pages 117–122, 2001.
- [10] D. E. Koditschek and E. Rimon. Robot navigation functions on manifolds with boundary. *Advances Appl. Math.*, 11:412–442, 1990.
- [11] S. G. Loizou and K. J. Kyriakopoulos. Closed loop navigation for multiple holonomic vehicles. *Proc. of IEEE/RSJ Int. Conf. on Intelligent Robots and Systems*, pages 2861–2866, 2002.
- [12] S.G. Loizou and K.J. Kyriakopoulos. Multi-robot navigation functions. *submitted*, 2004.
- [13] G. Muskato. Soft computing techniques for the control of walking robots. *Journal of Computing and Control Engineering*, pages 193–200, 1998.
- [14] R. Pirez, A. Lal, Y. Miyahara, J.-M. Breguet, and H. Bleuler. Modelling, characterisation and implementation of a monolithic piezo actuator (mpa) of 2 and 3 degrees of freedom (dof). *Actuator 2002*, 2002. Bremen, Germany.
- [15] E. Rimon and D. E. Koditschek. Exact robot navigation using artificial potential functions. *IEEE Trans. on Robotics and Automation*, 8(5):501–518, 1992.
- [16] L. Sun, M. Li, and Y. Chu. Control system of mobile micro-robot based on dsp. *Int. Conf. on Electrical machines and systems ICEMS*, pages 495–497, 2003.
- [17] Y. Wen, G. Lu, and X. Zhao. Intelligent control method on primitive in micro-operation robot. *Proc. IEEE Robotics, Intelligent Systems and Signal Processing*, pages 1002–1006, 2003.
- [18] H. Wörn, F. Schmoekkel, A. Buerkle, J. Samitier, M. Puig-Vidal, S. Johansson, U. Simu, J. Meyer, and M. Biehl. From decimeter- to centimeter-sized mobile microrobots the development of the miniman system. *SPIEs Int. Symp. on Intelligent Systems & Advanced Manufacturing, Conference on Microrobotics and Microassembly*, 2001.
- [19] W. Zesch. *Multi-Degree-of-Freedom Micropositioning Using Stepping Principles*. PhD thesis, ETH Zurich, 1997.
- [20] <http://microrobotics.ira.uka.de/>. visited, 2005.